BBA - Bioenergetics 1859 (2018) 215–225

Contents lists available at ScienceDirect

BBA - Bioenergetics

journal homepage: www.elsevier.com/locate/bbabio

Probing the local lipid environment of the *Rhodobacter sphaeroides* cytochrome bc_1 and *Synechocystis* sp. PCC 6803 cytochrome b_6f complexes with styrene maleic acid

David J.K. Swainsbury[a], Matthew S. Proctor[a], Andrew Hitchcock[a], Michaël L. Cartron[a], Pu Qian[a], Elizabeth C. Martin[a], Philip J. Jackson[a,b], Jeppe Madsen[c], Steven P. Armes[c], C. Neil Hunter[a,*]

[a] Department of Molecular Biology and Biotechnology, University of Sheffield, Firth Court, Western Bank, Sheffield S10 2TN, United Kingdom
[b] ChELSI Institute, Department of Chemical and Biological Engineering, University of Sheffield, Sir Robert Hadfield Building, Mappin Street, Sheffield S1 3JD, United Kingdom
[c] Department of Chemistry, University of Sheffield, Brook Hill, Sheffield S3 7HF, United Kingdom

ARTICLE INFO

Keywords:
SMA
Cytochrome bc_1
Cytochrome b_6f
Rba. sphaeroides
Synechocystis
Quinone pool

ABSTRACT

Intracytoplasmic vesicles (chromatophores) in the photosynthetic bacterium *Rhodobacter sphaeroides* represent a minimal structural and functional unit for absorbing photons and utilising their energy for the generation of ATP. The cytochrome bc_1 complex (cytbc_1) is one of the four major components of the chromatophore alongside the reaction centre-light harvesting 1-PufX core complex (RC-LH1-PufX), the light-harvesting 2 complex (LH2), and ATP synthase. Although the membrane organisation of these complexes is known, their local lipid environments have not been investigated. Here we utilise poly(styrene-*alt*-maleic acid) (SMA) co-polymers as a tool to simultaneously determine the local lipid environments of the RC-LH1-PufX, LH2 and cytbc_1 complexes. SMA has previously been reported to effectively solubilise complexes in lipid-rich membrane regions whilst leaving lipid-poor ordered protein arrays intact. Here we show that SMA solubilises cytbc_1 complexes with an efficiency of nearly 70%, whereas solubilisation of RC-LH1-PufX and LH2 was only 10% and 22% respectively. This high susceptibility of cytbc_1 to SMA solubilisation is consistent with this complex residing in a locally lipid-rich region. SMA solubilised cytbc_1 complexes retain their native dimeric structure and co-purify with 56 ± 6 phospholipids from the chromatophore membrane. We extended this approach to the model cyanobacterium *Synechocystis* sp. PCC 6803, and show that the cytochrome b_6f complex (cytb_6f) and Photosystem II (PSII) complexes are susceptible to SMA solubilisation, suggesting they also reside in lipid-rich environments. Thus, lipid-rich membrane regions could be a general requirement for cytbc_1/cytb_6f complexes, providing a favourable local solvent to promote rapid quinol/quinone binding and release at the Q_0 and Q_i sites.

1. Introduction

Intracytoplasmic vesicles (chromatophores) in the photosynthetic bacterium *Rhodobacter* (*Rba.*) *sphaeroides* (Fig. 1A) are spherical invaginations of the membrane. These structures represent a minimal structural and functional unit for absorbing photons and utilising their energy to produce ATP via an efficient energy generation mechanism [1,2]. The cytochrome bc_1 complex (cytbc_1) is one of the four major components of the chromatophore alongside the reaction centre-light harvesting 1-PufX core complex (RC-LH1-PufX), the light-harvesting 2 complex (LH2), and ATP synthase [1]. The stoichiometry and organisation of these complexes, revealed by mass spectrometry and atomic force microscopy (AFM) [1,3], appears to be optimised for photosynthetic growth at low light intensities, below 50 μmol m^{-2} s^{-1} [1,2,4], when *Rba. sphaeroides* cells contain up to 1500 intracytoplasmic vesicles [5], observed both as single and budded structures [6,7]. Chromatophores house short rows of dimeric RC-LH1-PufX complexes surrounded by tens of LH2 complexes [1,2], which provide a

Abbreviations: Rba. sphaeroides, *Rhodobacter sphaeroides*; cytbc_1, cytochrome bc_1 complex; cytb_6f, cytochrome b_6f complex; RC-LH1-PufX, reaction centre light harvesting complex 1-PufX core; LH2, light harvesting 2 complex; UQ_{10}, ubiquinone 10; cytc_2, cytochrome c_2; PMF, proton motive force; AFM, atomic force microscopy; TEM, transmission electron microscopy; *Synechocystis*, *Synechocystis* sp. PCC 6803; PSI, photosystem I; PSII, photosystem II; SMA, poly(styrene-*alt*-maleic acid); SMALPs, styrene-maleic acid lipid particles; β-DDM, *n*-Dodecyl-beta-Maltoside; M_w, Mass average molecular weight; WT, wild-type; CV, column volume; TLC, thin layer chromatography; HPLC, high performance liquid chromatography; PG, phosphatidylglycerol; PE, phosphatidylethanolamine; CL, cardiolipin; PC, phosphatidylcholine; SQDG, sulfoquinovosyl diacylglycerol

* Corresponding author.
E-mail address: c.n.hunter@sheffield.ac.uk (C.N. Hunter).

https://doi.org/10.1016/j.bbabio.2017.12.005
Received 16 October 2017; Received in revised form 21 December 2017; Accepted 28 December 2017
Available online 29 December 2017

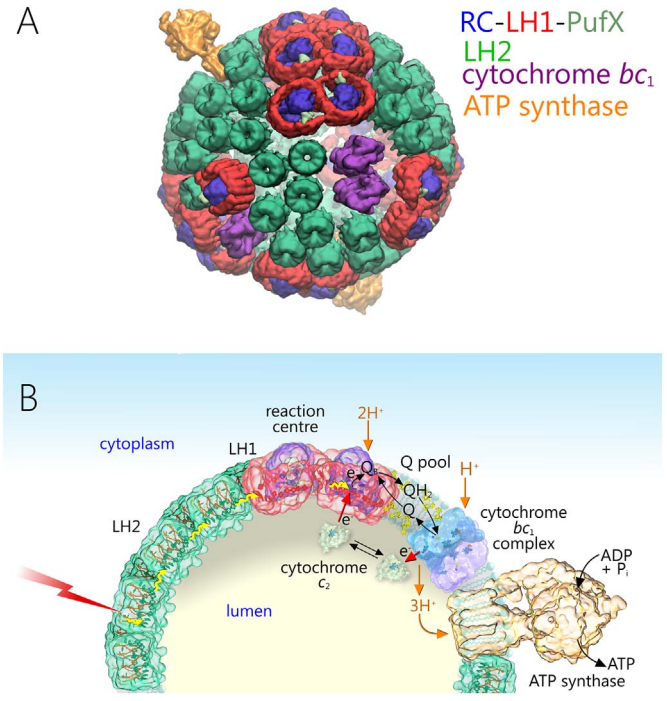

Fig. 1. A: Molecular model of the chromatophore comprised of LH2 (green), LH1 (red), PufX (beige), the reaction centre (RC, blue), cytbc_1 (purple) and ATP synthase (yellow). This figure was produced from a model featured in refs [1,2]. B: Schematic representation of LH2, RC-LH1-PufX and cytbc_1 as a cross-section of part of the chromatophore vesicle in panel A. Two successive photons (red) incident on an LH2 complex, then excitation energy transfer (wavy yellow arrows) to LH1 then a RC, drives two charge separations eventually producing a quinol (QH_2), which migrates via the quinone pool to a nearby cytbc_1 complex. Electron holes at the RC are filled by reduced cytc_2 which receives electrons from the cytbc_1 complex (red arrows), completing this cyclic electron transfer process. These protons are finally utilised by the ATP synthase to generate ATP from ADP and inorganic phosphate (P_i). Diffusion of mobile electron carriers at the membrane surface and Q/QH_2 within the membrane bilayer are shown with black arrows. Orange arrows denote movement of protons; for every four turnovers at the RC, six protons accumulate in the lumen; the diagram shows the average for two RC turnovers, i.e. for each quinol produced.

variable antenna that can adjust to changeable light levels [5]. Close packing between these complexes promotes rapid and efficient energy transfer and trapping. The overall trapping time of ~60 ps [8] is accounted for by energy migration between LH2 complexes, and from LH2 to LH1, on a picosecond timescale [9–11]. Transfer from the encircling LH1 ring to the special pair (P) BChl dimer within the RC (Fig. 1B) [12] drives picosecond charge separation within the RC [13].

Following two rounds of charge separation, and re-reduction of oxidised P (Fig. 1B, red arrow) by cytochrome c_2 (cytc_2), a ubiquinone-10 (UQ_{10}) molecule bound to the Q_B site becomes fully reduced, and binds two protons from the cytoplasm to generate a quinol (Fig. 1B) (see [13] for a comprehensive review of the RC). The reduced quinol leaves the RC, traverses the surrounding LH1 antenna through a pore created by the PufX polypeptide [14], and diffuses within the membrane to the cytbc_1 complex [15] via the free quinone pool (Fig. 1B black arrows). The cytbc_1 generates a proton motive force (PMF) via a modified Q-cycle [16] in which quinol binds to the Q_0 site releasing two protons into the lumen of the chromatophore (Fig. 1B orange arrows). One electron is transferred along the high potential chain via the Rieske Fe-S subunit to reduce an oxidised cytc_2, which diffuses to a photo-oxidised RC to reduce P, completing the cyclic electron transfer chain. The second electron enters the low potential chain via two *b*-type cytochromes to reduce a second UQ_{10} molecule bound at the Q_i site. Arrival of another quinol and a repeat of the above reactions generates an 'extra' quinol at the Q_i site, so this Q-cycle mechanism effectively amplifies the yield of protons for each absorbed photon [16]. The PMF generated by these processes is utilised by ATP synthase to generate ATP from ADP and inorganic phosphate. There are approximately 4 cytbc_1 complex dimers present in each chromatophore, and this number is rate limiting for photosynthetic ATP formation [1,2].

Cartron et al. [1] demonstrated that dimeric cytbc_1 complexes and dimeric RC-LH1-PufX complexes are found in close proximity, but not necessarily in direct contact, an arrangement that minimises the cycling time for diffusion of Q/QH_2 and cytc_2 between them. It was also shown that the cytbc_1 complex was much more susceptible to detergent solubilisation than RC-LH1-PufX and LH2, suggesting that its local environment may be lipid-rich, consistent with a proposed quinone- and lipid-rich phase surrounding the cytbc_1 complexes [17]. The cytochrome b_6f (cytb_6f) complex in cyanobacteria, algae and plants [18], which performs an analogous function to cytbc_1 in purple bacteria, could also sit in a lipid- and quinone-rich nanoenvironment. AFM of plant thylakoids showed that cytb_6f complexes are found within 20 nm of photosystem II (PSII) RCs, again consistent with predictions from kinetic studies showing confinement of quinones within the local PSII-cytb_6f environment [19–21].

New approaches are required to characterise the membrane environments of the photosynthetic complexes described, and poly (styrene-*alt*-maleic acid) (SMA) co-polymers represent one such tool. In recent years there has been growing interest in SMA for membrane-protein solubilisation; once converted to the acid form 2:1 or 3:1 styrene to maleic-acid ratio polymers can effectively solubilise biological membranes and their constituent protein complexes [22–27]. Unlike detergents, SMAs do not remove the annular lipids of membrane protein complexes, instead forming nanodiscs in which the protein is embedded in a belt of lipids from the source membrane stabilised by the polymer. These structures are termed native nanodiscs or styrene-maleic acid lipid particles (SMALPs) and have been found to improve the stability of complexes as well as give more native-like biophysical properties when compared to preparations using detergents [22,23,28–33]. The resultant SMALPs are amenable to both biophysical analysis and characterisation of the co-purified lipids, providing insight into the local lipid environments of the proteins within [28,31,34]. A recent investigation of the properties of SMA has revealed that these polymers effectively preserve even weak protein-protein contacts, such as those involved in formation of RC-LH1-PufX arrays, allowing for enrichment of native large-scale protein architectures [27]. To this end we have utilised SMA as a tool to probe the local lipid environment of the RC-LH1-PufX, LH2 and cytbc_1 complexes from *Rba. sphaeroides* chromatophores. As hypothesised by previous studies we find that the cytbc_1 complex resides in a lipid-rich environment whereas the RC-LH1-PufX and LH2 complexes reside in relatively lipid-poor domains. By purifying cytbc_1 SMALPs we further characterised the local lipid environment of this complex. We extended this methodology to membranes of the model oxygenic photosynthetic cyanobacterium *Synechocystis* sp. PCC 6803 and find that the PSII and cytb_6f complexes are highly susceptible to SMA solubilisation, indicating they also reside in lipid-rich environments. Together these data suggest that lipid-rich membrane regions provide a favourable local solvent to promote rapid quinol/quinone binding and release at the Q_0 and Q_i sites of cytbc_1 and cytb_6f complexes.

2. Materials and methods

2.1. Preparation of SMA

Xiran SZ30010 polystyrene-maleic anhydride (2:1 ratio styrene to maleic anhydride, 10 kDa mass average molecular weight (M_w)) was a generous gift from Polyscope EU. The polymer was converted to the acid form by refluxing in excess KOH as previously described [27] at a concentration of 5% w/v. The pH was adjusted to 8.0 with solid KOH prior to use to avoid dilution of the solution.

2.2. Growth of Rba. sphaeroides

The construction and growth of a *Rba. sphaeroides* mutant containing a His_{10} tagged cytbc_1 c-subunit (PetC) was described previously [1]. For solubilisation assays cells were grown in M22+ medium either photosynthetically in 1 L of medium with illumination from ORSAM CLASSIC 116 W halogen light bulbs under "medium light" (approximately 100 μmol m^{-2} s^{-1} illumination for 16 h) or "low light" (approximately 30 μmol m^{-2} s^{-1} illumination for 48 h) conditions, or semi-aerobically in 1.6 L of medium in the dark for 48 h. Cells (8 L) for protein preparations were grown photosynthetically under approximately 30 μmol m^{-2} s^{-1} illumination for 72 h. Cells were harvested by centrifugation at 4000 RCF for 20 min and stored at − 20°C until required.

2.3. Generation of histidine-tagged cytb_6f in Synechocystis sp. PCC 6803

A DNA sequence encoding the thrombin cleavable His_{10} tag from pET52b (Novagen) was added in frame to the end of the *petA* gene (sll1317), which encodes apocytochrome *f*. This is the same tag added to the C-terminus of the *Rba. sphaeroides* cytochrome c_1 component of the cytbc_1 complex described in Section 2.2 [1]. The tag was followed by a stop codon and the first 25 bp of the chloramphenicol acetyl transferase (*cat*) cassette from pACYC184. This construct was synthesised (Integrated DNA Technologies) and the *cat* cassette and 500 bp of DNA immediately downstream of the *petA* gene were amplified separately by PCR, from pACYC184 with primers catF/catR or from *Synechocystis* sp. PCC 6803 genomic DNA with primers petA_ds_F/petA_ds_R, respectively. These three fragments were joined by overlap extension PCR using primers petA_F and petA_ds_R, and the resulting product was cloned into the *Bam*HI and *Hin*dIII sites of pUC18. The sequence verified (GATC Biotech) fragment was excised with *Bam*HI/*Hin*dIII and introduced to wild-type (WT) *Synechocystis* as described previously [35]. Tranformants were selected using 5 μg mL^{-1} chloramphenicol and genome copies segregated by sequential doubling of the antibiotic concentration to 40 μg mL^{-1}. Segregation was confirmed by PCR screening with oligos petA_screen_F and petA_screen_R, resulting in a product of 1941 bp for transformants, compared to 1076 bp in the WT. The *petA* locus amplified from transformant genomic DNA was sequenced to ensure the His-tag was in frame with the *petA* gene.

2.4. Preparation of Rba. sphaeroides chromatophore membranes

Cells were suspended in 20 mM Tris pH 8 containing a few crystals of DNAse1 and Roche complete EDTA-free protease inhibitors. Cells were lysed either by two passes through a French press (AminCo, USA), or a single pass through a cell disruptor (Constant systems), both at 20000 PSI. Insoluble material was removed by centrifugation at 18459 RCF (avg) for 15 min at 4 °C. Soluble material was loaded onto 40/15% w/w sucrose step gradients and centrifuged at 107400 RCF (avg) for 10 h at 4 °C. Membranes were harvested from the 40–15% sucrose solution interface and stored in aliquots at − 20 °C.

2.5. Preparation of Synechocystis sp. PCC 6803 thylakoid membranes

Synechocystis sp. PCC 6803 cells producing C-terminally His-tagged apocytochrome *f* were grown to an optical density (OD) at 750 nm of approximately 1 in a volume of 16 L BG11 [36] medium with aeration and 100 μmol m^{-2} s^{-1} illumination from ORSAM CLASSIC 116 W halogen light bulbs at room temperature (approximately 21 °C) and harvested by centrifugation at 17700 RCF (avg) at 4 °C for 20 min. Pellets from 8 L of culture were washed and re-suspended in thylakoid buffer (25 mM sodium phosphate pH 7.4, 5 mM $MgCl_2$ and 200 mM NaCl and complete EDTA-free protease inhibitors [Roche]) and mixed with an equal volume of 0.1 mm glass beads (BioSpec).

To prepare membranes for SMA solubilisation assays the cells were broken in a Mini-Beadbeater-16 (BioSpec) for eight 20 s cycles with samples cooled on ice between each cycle. The cell lysate was pelleted at 38000 RCF (avg) at 4 °C for 30 min before being re-suspended in thylakoid buffer. Aliquots of 3 mL cell lysate were loaded onto multiple sucrose step gradients consisting of 2 mL 50% w/w sucrose and 8 mL 30% w/w sucrose and centrifuged for 30 min at 111000 RCF (avg) in a Beckman SW41 Ti rotor for 1 h at 4 °C. The bands containing thylakoid membranes were harvested from the interface between the 30 and 50% sucrose steps.

To prepare membranes for the purification of His_{10}-tagged cytb_6f, the cells were broken by bead beating using ten 55 s cycles. Soluble and membrane proteins were separated by centrifugation at 38000 RCF (avg) at 4 °C for 30 min and the membranes were resuspended in 100 mL 20 mM Tris pH 8 containing 200 mM NaCl.

2.6. Solubilisation assays

The solubilisation assay was adapted from the method described by Swainsbury et al. [27]. 2 mL *Rba. sphaeroides* membranes with an OD_{850} of 3 (1 cm pathlength) were prepared in solutions of 20 mM Tris pH 8 containing 200 mM NaCl and either 2.5% w/v SMA, 3% w/v *n*-Dodecyl-beta-Maltoside Detergent (β-DDM) or without solubilising agents. *Synechocystis* sp. PCC 6803 membranes were solubilised at OD 5 (680 nm, 1 cm pathlength) in 25 mM sodium phosphate buffer pH 7.4 containing 200 mM NaCl, 5 mM $MgCl_2$ and 2.5% w/v SMA in a total volume of 2 mL. Samples were incubated at room temperature in the dark for 1 h.

A volume of 1 mL was centrifuged at 100000 RCF (avg) for 2 h at 4 °C. After this, 0.9 mL was removed with care taken not to disturb the pellet; this sample will be termed the "soluble fraction". The remaining 1 mL of each sample, hereafter referred to as the "total fraction", was stored at 4 °C in the dark until required.

Spectra of the "total" and "soluble" fractions were collected in the short (0.33 cm) path of a quartz semi-micro cuvette between 1000 and 400 nm. Samples were then transferred into 1 mL disposable cuvettes and spectra were collected before and after the addition of a few grains of sodium dithionite.

Spectra collected in the 0.33 cm path were processed by scatter correcting and deconvoluting the contributions of RC-LH1-PufX and LH2 using a modified version of an Excel spreadsheet by available at https://terpconnect.umd.edu/~toh/spectrum/CurveFittingB.html. The spreadsheet adds spectra of the two complexes and a scatter curve to achieve a best fit to the data and returns spectra for the three components according to their fitted contributions. The scatter curve used was calculated using $\lambda^{-2.6}$, and the RC-LH1-PufX and LH2 reference spectra were produced from proteins purified as described elsewhere [37,38]. The reference spectra used are shown normalised to their maxima in Supplementary Fig. 1 panel E. The extraction efficiency of RC-LH1-PufX and LH2 was calculated from the difference in absorbance at 875 and 850 nm respectively, in the "total" and "soluble" fractions. The 1 cm pathlength spectra were processed by generating oxidised minus reduced spectra and using the difference at 560 nm between the "total" and "soluble" fractions to estimate extraction efficiency of the cytbc_1 complex.

For *Synechocystis* sp. PCC 6803 membranes the same procedure was used, except samples had an OD_{680} of 5; the short pathlength UV/Vis spectra were collected in a 0.2 cm quartz cuvette and reference spectra for PSI and PSII were used for deconvolution using the procedure described above for RC-LH1-PufX and LH2 using the reference spectra presented in Supplementary Fig. 5C [39].

The extractions of cytbc_1 and cytb_6f were also estimated by haem blot [40]. 20 μl volumes from "soluble" and "total" fractions were separated on SDS-PAGE gels, transferred to a polyvinylidene difluoride (PVDF) membrane and the cytochrome *c*/*f* subunits were visualised using Westar 2.0 solution (Cyanagen). Band intensities were integrated using ImageJ [41] and extraction efficiencies were

calculated by comparison of the band intensity of "total" and "soluble" fractions.

2.7. Native PAGE electrophoresis

Synechocystis sp. PCC 6803 membranes with an OD_{680} of 6, 12 and 24 were solubilised in 2.5% w/v SMA as described in Section 2.6. 15 μL of each sample was incubated in 4% w/v β-DDM for 1 h at room temperature in the dark. Samples were then diluted 2-fold in either clear native buffer (125 mM Tris pH 6.8, 30% glycerol) or blue native buffer (125 mM Tris pH 6.8, 30% v/v glycerol, 0.01% w/v bromophenol blue). Samples were run on NuPAGE Tris-acetate 3–8% gels (Novex) at 150 v for ~2 h. For clear native page the upper buffer was supplemented with 0.05% w/v deoxycholate and 0.04% w/v β-DDM and blue native gels were supplemented with 1 mL blue native additive.

Gels were imaged using an Amasham Imager 600 in colour. Clear native gels were also imaged by fluorescence with excitation at 460 nm monitoring emission using the cy5 filter with 12 s exposure. Bands were assigned according to [42].

2.8. Purification of cytbc_1 and cytb_6f complexes

Membranes from a 4 L culture of photosynthetically grown *Rba. sphaeroides* cells or 8 L *Synechocystis* sp. PCC 6803 cells were solubilised in 20 mM Tris pH 8 containing 200 mM NaCl and 1.5% w/v SMA at room temperature for 1 h in the dark. Insoluble material was removed by centrifugation at 113000 RCF (avg) for 1 h at 4 °C. Solubilised cytbc_1 or cytb_6f complexes were bound to a 20 mL HisPrep FF Ni-NTA column (GE Healthcare) pre-equilibrated with 5 column volumes (CV) binding buffer (20 mM Tris pH 8 containing 200 mM NaCl and 20 mM imidazole) by recycling overnight at 5 mL min^{-1}. The column was washed with 20 CV binding buffer followed by 10 CV binding buffer containing 40 mM imidazole. The cytbc_1 or cytb_6f complexes were eluted in 20 mM Tris pH 8 containing 200 mM NaCl and 250 mM imidazole. For *Rba. sphaeroides* cytbc_1 further purification and buffer exchange were performed by size-exclusion chromatography on a HiPrep Sephacryl 16/60 S-300 column (GE Healthcare) in 20 mM Tris pH 8 containing 200 mM NaCl. Fractions with an absorbance at 415 nm to absorbance at 280 nm ratio above 1.25 were concentrated and stored at −80 °C until required. The concentrations of cytbc_1 haem *b* and haem *c* in the preparation were determined using dithionite reduced samples with extinction coefficients of $\varepsilon_{561-575}$ of 22 mM^{-1} $cm^{-1}$and $\varepsilon_{551-540}$ of 19 mM^{-1} cm^{-1}, respectively, as described in [1].

2.9. Thin layer chromatography

Thin layer chromatography (TLC) was performed according to [43] with some modifications. Lipids were extracted from ~0.5 nmol cytbc_1 SMALPs or ~0.4 OD_{850} units of membranes in 50 μl 1:1 methanol: chloroform. Samples were loaded alongside pure lipid standards on Whatman Partsil Diamond LK6DF TLC plates. Plates were developed in either 85:15:10:3.5 or 85:25:10:3.5 chloroform:methanol:acetic acid:water (by volume) for 30 min. Lipids were visualised by incubating the plate in 50% v/v H_2SO_4 for 30 s followed by heating at 160 °C for 60 min. Plates were imaged and band intensities were integrated in Image J [41]. Data from both conditions were combined to give six data-sets for membranes and eight for SMALPs and all data were normalised to the intensity of the phosphatidylglycerol (PG) band.

2.10. Ubiquinone-10 quantification

Ubiquinone-10 (UQ_{10}) was quantified according to "Determination of Coenzyme Q10 by High Pressure Liquid Chromatography" customer application brief #101 by Dionex and the method in [44] with several modifications. Standards were prepared by dissolving pure UQ_{10} in 50:50 v/v chloroform:methanol containing 0.02% w/v ferric chloride. Lipids were extracted from 0.5 nmol cytbc_1 in the same solvent. Samples were analysed by high performance liquid chromatography (HPLC) using a Beckman Coulter ODS 4.6 mm × 2.5 cm C18 column and eluted at 1 mL min^{-1} in 80:20 v/v methanol:2-propanol over 45 min. Peaks at 29.5 and 32 min were integrated and used for calculations. Three samples of cytbc_1 were analysed and the calculated concentrations of UQ_{10} were averaged.

2.11. Lipid quantification

Phospholipids were quantified according to [1]. A total of 0.46 nmol cytbc_1 was dissolved in approximately 50 μl chloroform in pre-cleaned glass test-tubes. Phosphate standards were prepared using solutions of 0, 0.25, 0.5, 1, 5, 10, 20, 50, 75, 100 and 200 nMol KH_2PO_4 dissolved in 50 μL chloroform. All samples were dried at 140 °C for 20 min. Lipids were hydrolysed by adding 0.15 mL perchloric acid and incubating at 180 °C for 2 h. Phosphate was visualised colourimetrically by adding 0.5 mL H_2O, 1.25% w/v ammonium hepta-molybdate and 5% w/v 0.2 mL ascorbic acid followed by incubation at 100 °C for 5 min. Spectra were collected and the absorbance at 800 nm was used to determine phosphate concentrations.

2.12. Preparation of nanogold labelled membranes

Membranes were labelled with nanogold according to Cartron et al. [1]. Membranes (OD_{850} of 10) were incubated for 1 h in 20 mM Tris pH 8, or 20 mM Tris pH 8 containing 0.02% w/v β-DDM or 2.5% w/v SMA for 1 h in a final volume of 2.4 mL. After incubation, 0.6 mL 0.5 mM 5 nm Ni-NTA-Nanogold (Nanoprobes) was added and samples were incubated for an additional 1 h. Samples were loaded onto gradients of 50/40/30/20/15% w/v sucrose in 20 mM Tris pH 8 and centrifuged at 178305 RCF (avg) for 2 h at 4 °C. Fractions were collected from the gradients in 1 mL volumes with a peristaltic pump and spectra were collected between 400 and 1000 nm. A second set of membranes was prepared as above without the addition of nanogold. The relative cytbc_1 content of gradient fractions was estimated by haem blot as described for solubilisation assays (Section 2.6).

2.13. Transmission electron microscopy

Samples, either 5 μL 1 μM cytbc_1 or OD_{850} 0.3 membranes, were incubated on glow-discharged carbon-coated copper grids for 30 s followed by washing with deionised water and staining with 0.75% w/v uranyl formate for 30 s. Grids were imaged in a Phillips CM100 TEM equipped with a Gatan Ultrascan 667 camera at between 27000 and 52000 × magnification.

2.14. Dynamic light scattering

Solutions containing 1 μM cytbc_1 were prepared in 20 mM Tris pH 8 containing 200 mM NaCl and aggregates were removed by centrifugation at 15000 RCF in a benchtop centrifuge for 10 min. Samples were filtered through a 0.2 μm syringe filter prior to measurement in a Zitasizer nano ZS in a 1 mL cuvette collecting three sets of ten × 10 s measurements at 25 °C.

3. Results

3.1. Solubilisation of chromatophore membranes with SMA

SMA has been shown to preferentially solubilise proteins within lipid-rich membrane environments whilst leaving lipid-poor domains, such as densely packed antenna arrays, intact [27]. In order to probe the local lipid environment of the cytbc_1 complex we performed solubilisation trials with SMA and measured its ability to solubilise RC-LH1-PufX, LH2 and cytbc_1. We selected 10 kDa M_w SMA with a 2:1 styrene to

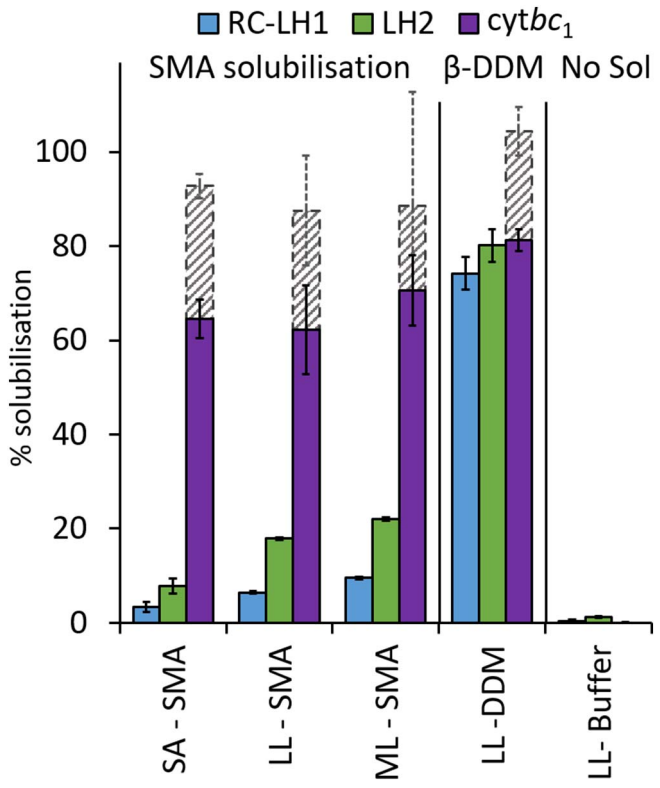

Fig. 2. Extraction efficiencies of RC-LH1-PufX (blue), LH2 (green) and the cytbc_1 complex (magenta) in membranes prepared from cells grown under semi-aerobic (SA), or low light (LL) and medium light (ML) photosynthetic conditions. The left panel shows solubilisations in 2.5% w/v SMA, the centre panel shows low light membranes solubilised in 3% w/v β-DDM, and the right panel shows results where no solubilising agents were added. Solid bars show values obtained by spectroscopy and hatched bars show values for cytc_1 by haem staining. Error bars show standard error of the mean for three replicates.

maleic acid ratio for this study. This polymer has previously been shown to efficiently solubilise proteins residing in lipid-rich environments from in *Rba. sphaeroides* membranes whereas RC-LH1-PufX arrays are left intact [27]. Thus, this SMA should allow the best possible discrimination of lipid-rich and lipid-poor domains. As the level of LH2 expression can affect the morphology of chromatophore membranes, solubilisation trials were performed on membranes prepared from cells grown either semi-aerobically in the dark, or photosynthetically under ~30 μmol m^{-2} s^{-1} (low light) for 48 h, or ~100 μmol m^{-2} s^{-1} (medium light) for 16 h. By deconvolution of the spectra the molar ratios of LH2 to RC-LH1-PufX in these membranes were estimated to be 2.5:1, 2.4:1 and 2.0:1, respectively.

To estimate the percentage of each complex extracted, UV/Vis spectra of SMA solubilised membranes were collected before and after ultracentrifugation. The contributions of RC-LH1-PufX and LH2 complexes, and of light scattering, were deconvoluted by fitting spectra of pure complexes and a calculated scatter curve to a spectrum of the SMA treated chromatophores. Example spectra and their deconvoluted components are shown in Supplementary Fig. 1. The deconvoluted spectra were used to estimate the solubilisation efficiencies for RC-LH1-PufX and LH2, shown in Fig. 2 with blue and green bars respectively, calculated by the differences in absorbance before and after removal of the insoluble material. The solubilisation of cytbc_1 was estimated by comparing the change in absorbance at 560 nm upon dithionite treatment before and after ultracentrifugation (Fig. 2, magenta bars). A second estimate was made by detection of the covalently linked *c*-type cytochrome of the 30 kDa cytc_1 subunit by haem staining [40] and comparing the intensity of the bands in the total and soluble fractions (Fig. 2, shaded bars). Example haem blots and difference spectra are shown in Supplementary Fig. 2. These blots also contained a 24 kDa band, consistent with the apparent mass of the membrane-associated cytc_y [45], which was omitted from these calculations.

Treatment of chromatophore membranes with 2.5% w/v SMA revealed that the major photosynthetic complexes are not solubilised with uniform efficiency. As shown in Fig. 2, the RC-LH1-PufX complexes are highly resistant to SMA solubilisation, and are extracted with 3.3 ± 1.1% efficiency from membranes from semi-aerobically grown cells. This value is similar to that previously determined by Swainsbury et al. [27] for RC-LH1-PufX containing membranes lacking LH2 from cells grown under the same conditions. The low solubilisation efficiency arises because SMA is unable to disrupt the highly ordered and closely packed arrays formed by these complexes [27]. The solubilisation efficiency increases slightly in membranes from low and medium light grown cells at 6.4 ± 0.2 and 9.5 ± 0.3%, respectively. The LH2 complex is slightly less resistant to SMA solubilisation with efficiencies of 7.8 ± 1.7, 17.9 ± 0.3 and 22.0 ± 0.4% for membranes from semi aerobically grown, low light and medium light grown cells, respectively. This level of LH2 solubilisation is similar to that in trials performed on membranes from strains lacking the RC-LH1-PufX complex (data not shown). It should be noted that the increase in solubilisation efficiency correlates with the reduction of the LH2 to RC-LH1-PufX ratio. This is presumably a consequence of the somewhat different arrangements of the RC-LH1-PufX and LH2 within these membranes. Estimated solubilisation of cytbc_1 was much more efficient at 64 ± 4, 62 ± 9 and 70 ± 7% for semi aerobic, low light and medium light membranes respectively, as determined by reduced-oxidised spectra shown in Fig. 2 by the solid magenta bars (see Supplementary Fig. 2 for raw spectra). Haem blots also demonstrate that cytbc_1 is very effectively solubilised by SMA with estimated efficiencies of 92 ± 2, 87 ± 12 and 88 ± 24% for semi aerobic, low light and medium light membranes respectively, as shown by hatched bars in Fig. 2 (see Supplementary Fig. 2 for raw data). Additionally, there was no apparent trend in relation to the LH2 to RC-LH1-PufX ratio. To demonstrate that this effect is specific to SMA, control solubilisations were performed using 3% w/v β-DDM. Solubilisation efficiency was above 74% under all growth conditions for all complexes (only data from low light membranes are shown for clarity). In the absence of solubilising agents, solubilisation was < 2% for the RC-LH1-PufX and LH2 complexes and below the limit of detection for cytbc_1.

3.2. Characterisation of insoluble material after SMA treatment

To examine RC-LH1-PufX and LH2 after treatment of chromatophores with SMA, solubilisation mixtures were fractionated on sucrose density gradients then analysed by UV/Vis spectroscopy, haem blotting and negative-stain TEM imaging. For comparative purposes we also analysed chromatophores treated with sub-solubilising concentrations (0.02% w/v) of β-DDM to generate flattened membrane patches, which are more amenable to nanogold labelling and TEM imaging than untreated chromatophores [1]. This β-DDM concentration allows imaging of membrane patches containing all of their native complexes. Panel A in Fig. 3 shows sucrose gradients of *Rba. sphaeroides* chromatophores after these treatments. The untreated membranes form an abundant band at the 20/30% w/w sucrose interface (at the boundary of fractions 4 and 5 in Fig. 3A). After treatment with 0.02% w/v β-DDM this band is still present suggesting the membranes remain intact, although the band appears more diffuse suggesting the population has become more heterogeneous. After treatment in fully solubilising concentrations of SMA, a band remains at the 20/30% w/w sucrose interface, suggesting that much of the membrane remains intact after SMA solubilisation. These gradients were separated into 1 mL fractions, with fraction 1 being at the bottom and 11 at the top of the tube. The membrane bands (fraction 5 for all samples) have distinctive absorbance spectra for RC-LH1-PufX and LH2 demonstrating that the integrity of these complexes has been maintained. As shown in Fig. 3 panel B, haem blotting reveals that for the untreated and β-DDM-treated samples the cytc_1 subunit remained associated with the RC-LH1-PufX and LH2 containing membrane band (raw data are shown in Supplementary Fig. 3). However,

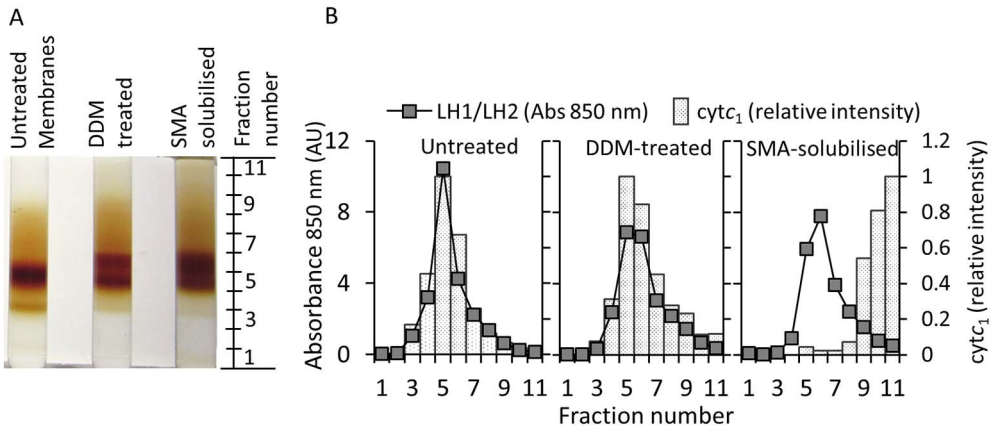

Fig. 3. A: Images of 15–50% w/w sucrose density gradients of untreated, 0.02% w/v β-DDM treated and SMA-solubilised chromatophore membranes. The scale on the right-hand side shows the approximate positions of the fractions taken from the gradient. B: UV/Vis absorbance profiles of fractions from the sucrose gradients shown in panel A. Absorbance of LH1/LH2 (squares connected by lines, based on absorbance at 850 nm) and relative intensities of the $cytc_1$ subunit from haem blots (bars) are shown.

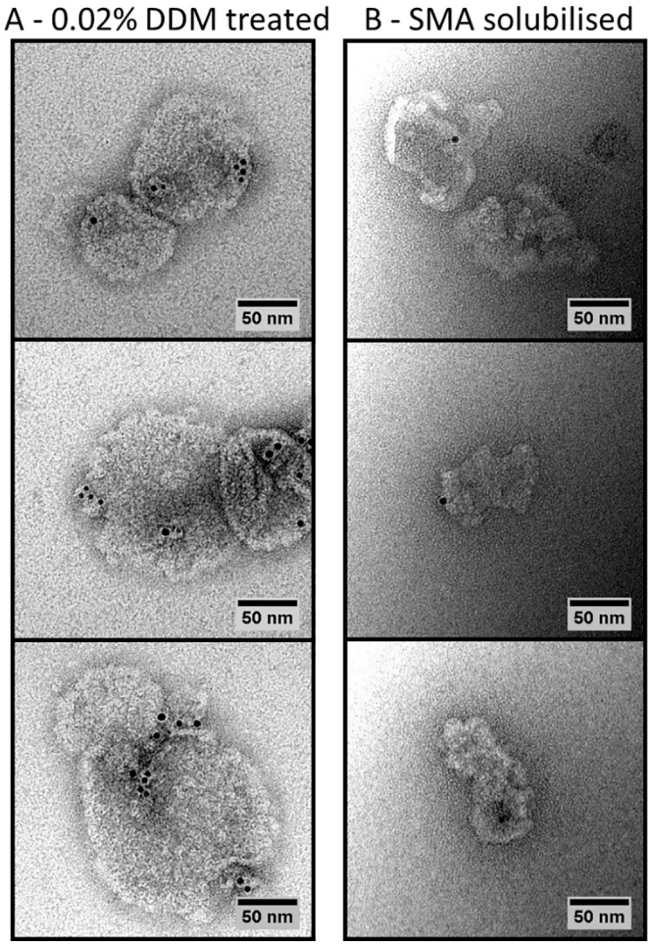

Fig. 4. Low resolution TEM images of typical membrane patches from nanogold-labelled chromatophores treated with 0.02% w/v β-DDM (A, left panels) or after complete solubilisation in 2.5% w/v SMA (B, right panels). Wide-field images are shown in Supplementary Fig. 4. Scale bars in the lower right of each image are 50 nm.

after SMA solubilisation the $cytc_1$ subunit is found in the upper portion of the gradient and no longer co-migrates with the remaining membrane material, showing that $cytbc_1$ has been solubilised and separated from the RC-LH1-PufX and LH2 complexes.

In a second set of gradients Ni-NTA nanogold was used to selectively label the His_{10} tag of the $cytbc_1$ complexes. As shown in Supplementary Fig. 4A, a significant band was observed at the 30/40% w/w interface, below the position of the major band in Fig. 3A at the 20/30% w/w interface, for untreated and β-DDM treated samples. Free nanogold migrated to the bottom of the tube (data not shown). For the SMA solubilised sample the lower band (40/30% interface) was very faint with the upper band (20/30% interface) being prominent, suggesting a reduced degree of membrane labelling. TEM images of grids prepared from each band revealed that the upper bands of untreated and β-DDM treated membranes contain mostly unlabelled circular objects with diameters of approximately 50 nm (shown in Supplementary Fig. 4B and C, zoomed images on the left show typical particles), consistent with the expected morphology of intact closed chromatophores. The lower band of the untreated membranes also contained similar structures with a low level of nanogold labelling, as shown in Supplementary Fig. 4D. In contrast the lower band of the β-DDM treated complexes contained large patches of 100–200 nm diameter (shown in Fig. 4A and Supplementary Fig. 4E), with multiple nanogold beads often appearing in pairs. Measurement of the patch area and number of nanogold beads gave a labelling density of 0.41 ± 0.19 beads per square micron (from 5 patches with an average area of 17500 ± 10400 μm^2; errors represent standard deviations of values for the individual patches). This result is consistent with the expected dimeric structure of the $cytbc_1$ complexes and is similar to images obtained by Cartron et al. [1] following the same sample preparation procedure. Together with the UV/Vis spectra we conclude that the membrane patches in the β-DDM-treated lower band are flattened chromatophores containing physiological quantities of $cytbc_1$ complexes. The TEM images of the SMA-solubilised and β-DDM treated samples are clearly different. Membrane patches in the upper band were smaller than those from the β-DDM treated samples at 50–100 nm in size and did not resemble intact chromatophores (shown in Fig. 4B and Supplementary Fig. 4E). These patches contained between 0 and 2 nanogold labels on average and each label was observed in isolation with a density of 0.17 ± 0.11 beads per square micron (from five patches with an average area of 5900 ± 1300 μm^2). The lower SMA band also contained 50–100 nm membrane patches, which had a slightly higher degree of nanogold labelling (0.3 ± 0.23 beads per square micron, from 5 patches with average area of 8100 ± 5200 μm^2) than the upper band, although this fraction accounted for only a minor proportion of the pigmented material. Together, data from the sucrose gradients in Fig. 3 and TEM imaging suggest that the majority of membrane fragments remaining after SMA solubilisation (seen in the upper SMA band, Fig. 4B) are smaller than those expected for flattened intact chromatophore membranes (DDM lower band, Fig. 4A), and have a greatly reduced $cytbc_1$ content. This is likely to be the result of preferential solubilisation of lipid-rich regions containing $cytbc_1$ by SMA, so they no longer co-migrate with the protein-rich RC-LH1-PufX and LH2 arrays (as shown in Fig. 3).

3.3. *Purification and characterisation of $cytbc_1$ SMALPs*

Multiple reports of solubilisation of proteins with SMA have demonstrated that the annular lipids of membrane complexes are co-

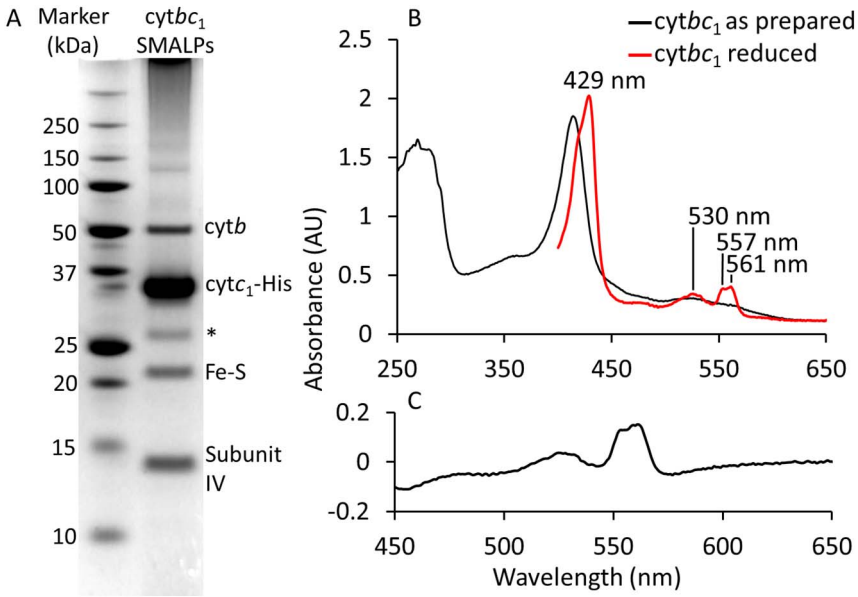

Fig. 5. A: SDS-PAGE gel of cytbc_1 SMALPs. * denotes a fifth contaminating band (see text). B: UV/Vis absorbance spectra of SMA purified cytbc_1 complexes either as prepared (black) or after reduction with sodium dithionite (red). Labels correspond to prominent peaks in the reduced spectrum. C: Reduced minus oxidised spectra calculated from spectra in panel B. The cytc_1 to cyt*b* ratio was calculated as 1.7:1 (see Materials and methods for details).

purified and amenable to analysis [28,31,34,46]. To this end we purified cytbc_1 SMALPs by nickel-affinity chromatography. Eluted fractions had a red colour and UV/Vis spectra revealed strong absorbance at 415 nm, which is indicative of haem containing proteins. Further purification by size exclusion chromatography removed residual RC-LH1-PufX and LH2, which eluted in the void volume. As shown in Fig. 5A, SDS-PAGE of purified cytbc_1 SMALPs revealed four major bands with masses corresponding to those of the cyt*b* (50 kDa), cytc_1-His (30.6 kDa), Rieske Fe-S (20 kDa) and Subunit IV (15 kDa) polypeptides [46]. A fifth faint band is observed at ~25 kDa; identification of the gel band by tryptic digestion and mass spectrometry showed that both cytc_1 (presumably a degradation product) and the zinc transporter ZnuC (UniProtKB ID: Q3IWB5) are present. ZnuC has a molecular weight of 26.5 kDa and eight histidine residues in its N-terminal 15 amino acids. This unusually high histidine content may give ZnuC a natural affinity for the nickel resin. Nevertheless, the lack of RC-LH1-PufX and LH2 in the final preparation demonstrates that the cytbc_1 complex has been effectively separated from the other major components of the chromatophore. Spectra of the pure complexes are shown in Fig. 5B and C. Upon reduction of the complexes with dithionite signals for both *b*- and *c*-type haems are observed. Analysis of reduced minus oxidised spectra estimated that the haem *b* to *c* ratio was 1.7:1 demonstrating that the cytbc_1 complexes are intact and fully functional.

TEM images of the purified cytbc_1 SMALPs (Fig. 6A) shows objects with a roughly elliptical shape. The average dimensions of the selected objects shown in the right-hand panels of Fig. 6A are 14 ± 2 × 9 ± 1 nm, roughly consistent with the size of the crystal structure of the *Rba. sphaeroides* cytbc_1 complex shown in Fig. 6B [47]. Analysis of the wide-field images (left) shows that larger structures are not present, demonstrating the preparation contains discrete cytbc_1 dimers rather than small membrane fragments, such as those in Fig. 4B. The presence of cytbc_1 dimers is further supported by dynamic light scattering of the cytbc_1 SMALPs, which detected particles with hydrodynamic diameters of 24 ± 10 nm corresponding to 97.9% of the material by mass.

As the cytbc_1 SMALPs are expected to contain lipids and quinones in addition to the identified polypeptides, analysis of the lipid content was performed. Thin layer chromatography of methanol/chloroform extracts of cytbc_1 SMALPs shows that five lipid species co-purified with the protein, identified as cardiolipin (CL), phosphatidylethanolamine (PE), phosphatidylglycerol (PG) and phosphatidylcholine (PC) by the matched migration of pure standards. The fifth lipid, sulfoquinovosyl diacylglycerol (SQDG), was assigned based on data from Swainsbury et al. [22,27] where the same five components were identified in *Rba. sphaeroides* RCs prepared from membranes lacking both LH1-PufX and LH2 complexes. It should be noted that recent publications on the rapid exchange of lipids in SMALPs suggest that conclusions cannot be drawn on particular lipid enrichment of the target complexes unless they are tightly bound to the protein [48,49]. Nevertheless, lipid extracts of bulk chromatophores show a similar lipid profile suggesting SMALP lipids originated from the source membrane and remained associated with the complex during preparation (Fig. 7). Quantification of the phospholipids estimates that there is an average of 56 ± 6 phospholipids per cytbc_1 dimer. To further characterise the co-purified membrane environment we used HPLC to show that 0.96 ± 0.18 UQ_{10} molecules are associated with each cytbc_1 complex. Pre-treatment of the membranes with antimycin A prior to purification yielded complexes where UQ_{10} was not detected (data not shown) suggesting any co-purified quinone is associated with the tight-binding Q_i site [47]. It should be noted that the aforementioned lipid exchange between SMALPs, or some as yet unexplored effect of SMA, may preclude enrichment of UQ_{10} molecules that natively reside within the lipid annulus of the cytbc_1 complex. This may explain why only a single, tightly bound UQ_{10} molecule was co-purified with each cytbc_1, but we also note that in the case of cytbc_1 there is no physical confinement of quinones by a defined protein environment surrounding the complex. In contrast, a pool of 10–15 UQ_{10} molecules/RC is sequestered within the solubilised and purified RC-LH1-PufX complex prepared using β-DDM [43], but in this case the quinones are effectively trapped between the RC and the encircling LH1 ring.

3.4. Extraction of cytb_6f from Synechocystis sp. PCC 6803 membranes

To further examine the ability of SMA to sample the lipid environments of complexes in photosynthetic membranes we attempted to replicate the study of *Rba. sphaeroides* cytbc_1 with the cytb_6f complex of the model freshwater cyanobacterium *Synechocystis* sp. PCC 6803 (hereafter *Synechocystis*). Using a procedure similar to the one described in Section 3.1, we found that SMA efficiently solubilises the cytb_6f complex. We estimated an extraction efficiency of 67 ± 11% by comparison of reduced minus oxidised spectra in total and soluble fractions, and 85 ± 2% by haem staining, as shown in Fig. 8A by the solid and hatched magenta bars, respectively (see Supplementary Fig. 5

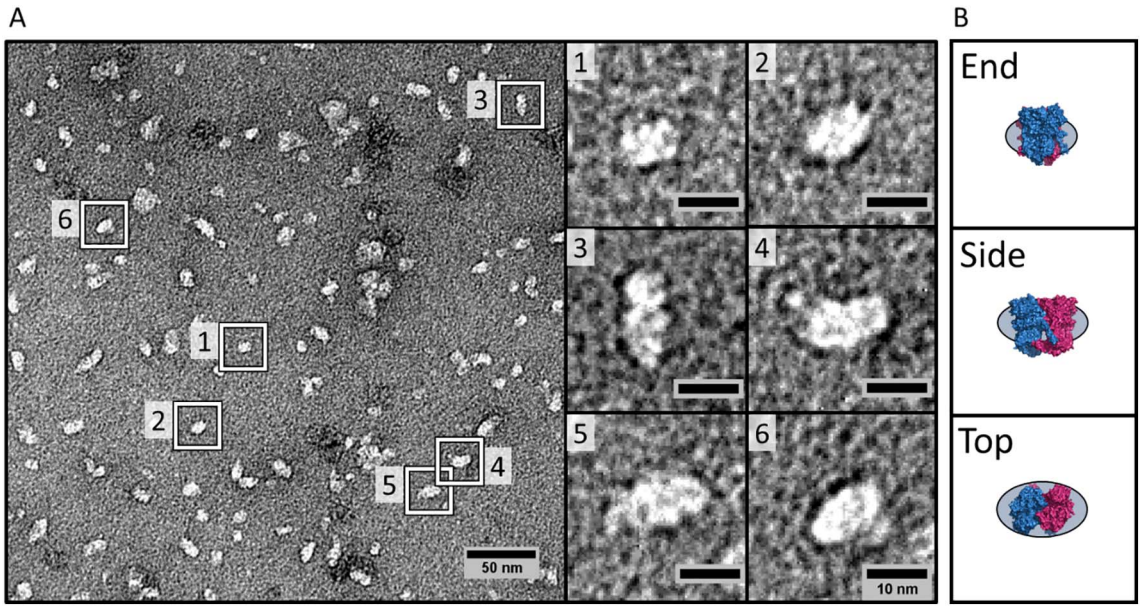

Fig. 6. Panel A: Negative stain TEM images of purified cytbc_1-SMALPs. Left: wide field image with selected complexes highlighted. Scale bar is 50 nm. Right: Zoomed images of six selected objects. The average dimensions were 14 ± 2 × 9 ± 1 nm. Inset scale bars are 10 nm. Panel B. Surface views of the cytbc_1 crystal structure [47] (PDB ID: 2QJP) from the end, side, or top. Images have been approximately scaled to match the sizes of zoomed objects in panel A. The two cytbc_1 monomers are shown in blue and red. Grey ovals show the area in which the lipid disc is expected to be located.

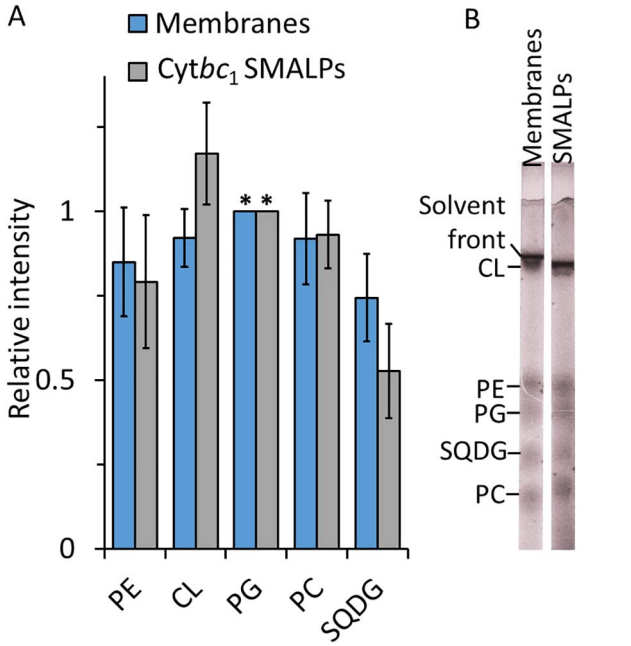

Fig. 7. Left panel (A): Lipid profiles of chromatophore membranes (blue) and cytbc_1-SMALPs (grey) determined by thin layer chromatography. Identified lipids were phosphatidylethanolamine (PE), cardiolipin (CL), phosphatidylglycerol (PG), phosphatidylcholine (PC) and sulfoquinovosyl diacylglycerol (SQDG). All band intensities are normalised to PG, labelled with asterisks. Error bars show standard error of the mean from seven (membranes) or eight (cytbc_1-SMALPs) samples. Right panel (B): Representative TLC lanes for membranes and cytbc_1-SMALPs.

for raw spectra). By deconvolution of the UV/Vis spectra of the total and soluble fractions following SMA treatment we could also estimate the extraction efficiency of both photosystems, PSI and PSII. This gave values of 2 ± 0.5% and 61 ± 11%, respectively (Fig. 8A, solid red and blue bars, and Supplementary Fig. 5). It should be noted that the values here are subject to large errors given their strongly overlapping absorption spectra. Nevertheless, as shown in Supplementary Fig. 5 panel D, the shift of the chlorophyll absorbance from 678 nm in the total fraction to 673 nm after removal of insoluble material clearly demonstrates that PSII is the dominant species solubilised by SMA whilst PSI mostly remains insoluble. This conclusion is supported by analysis of the soluble and total fractions by native PAGE. From blue native PAGE gels we observe that PSI complexes are depleted from the soluble fraction whereas PSII is not (Supplementary Fig. 5E). Fluorescence images of clear native PAGE gels also showed a strong signal for PSII in both the total and soluble fractions (Supplementary Fig. 5E). Integration of the fluorescence from three solubilisation trials gave an estimated PSII extraction efficiency of 58 ± 4% as shown in Fig. 8A by the blue hatched bar. This value is in good agreement with the estimate by deconvolution of the spectra.

To further analyse the solubilised cytb_6f complexes we enriched cytb_6f SMALPs by nickel-affinity chromatography. As shown in Fig. 8B the UV/Vis absorbance spectrum is typical of this complex showing a 670 nm chlorophyll peak, a strong haem Soret band at 420 nm and carotenoid absorbance between 400 and 550 nm [50]. Upon dithionite reduction two distinct peaks at 565 and 559 nm for the *b*- and *c*-type haems become apparent, suggesting that the cytb_6f complex is intact within SMALPs with all of its cofactors present. This spectrum matches that of pure cytb_6f reported previously [50]. These spectra also suggest that the cytb_6f complex does not co-purify with other pigmented components of the photosynthetic membranes as PSI or PSII absorbance features were not observed. We further analysed these complexes by negative stain TEM as shown in Fig. 8C. The typical wide-field image shown is free of large objects indicative of membrane patches or aggregates. The six zoomed objects, shown in the Fig. 6D, are consistent with cytb_6f viewed from multiple angles. The objects have average dimensions of 12 ± 3 × 8 ± 1 nm and are similar in shape to the roughly scaled images of the *Nostoc* sp. PCC 7120 crystal structure shown in Fig. 8E [51]. Taken together the analysis of the pure cytb_6f SMALPs shows that they are solubilised as discrete dimeric complexes rather than as part of larger membrane fragments. They also do not co-purify with other membrane proteins.

4. Discussion

SMA preferentially solubilises cytbc_1 complexes from *Rba. sphaeroides* chromatophore membranes, leaving RC-LH1-PufX and LH2

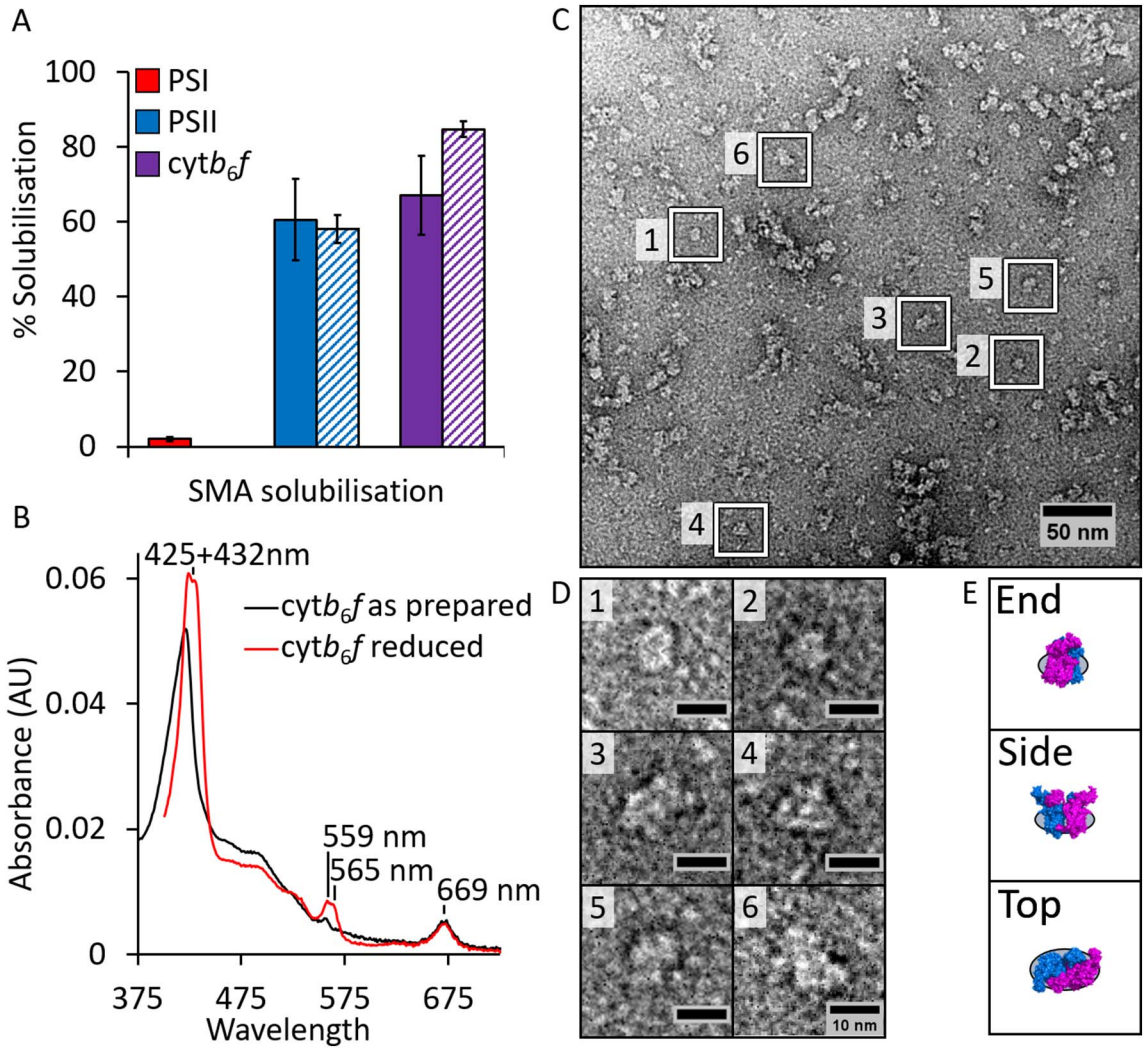

Fig. 8. Cytochrome b_6f extraction from *Synechocystis* thylakoids with SMA. (A): Estimated extraction efficiencies of PSI (solid red) and PSII (solid blue) from deconvoluted absorbance spectra. PSII solubilisation was also estimated from clear native page in-gel fluorescence (hatched blue bar). Solubilisation estimates for cytb_6f from reduced minus oxidised spectra and haem staining are shown with solid and hatched magenta bars, respectively. Error bars show standard errors of the mean. Raw data are shown in Supplementary Fig. 5. (B): UV/Vis spectra of purified cytb_6f either as prepared in buffer (black line) or after reduction with dithionite (red line). Labels show wavelengths of prominent peaks of the reduced spectrum. (C): Wide field negative stain TEM images of purified cytb_6f-SMALPs. (D): Zoomed images of selected complexes highlighted in panel C. Scale bar is 50 nm. The average dimensions were 12 ± 2 × 9 ± 1 nm. (E): Surface views of the cytb_6f crystal structure from *Nostoc* sp. PCC 7120 (PDB ID: 4OGQ) from the end, side and top. Images have been approximately scaled to match the sizes of zoomed objects in panel D. The two cytbc_1 monomers are shown in blue and pink. Grey ovals show the area in which the lipid-disc is expected to be located.

complexes largely unaffected. SMA acts efficiently on membrane complexes that sit in lipid-rich environments, as shown by work on several proteins including the bacterial SecYEG translocon and KcsA potassium channel [23,28]. Conversely, arrays of well-ordered and/or closely packed protein complexes such as RC-LH1-PufX and bacteriorhodopsin are poorly solubilised [27,52]. The liberation of cytbc_1 complexes from chromatophores by SMA fits with the proposed architecture of chromatophore membranes [1] in which LH2 and RC-LH1-PufX complexes form closely packed protein-rich arrays, whereas cytbc_1 complexes are found in lipid-rich regions of the membrane, which is ideal for the production of SMALPs due to the abundance of lipids from which a nanodisc can be formed.

There are several compelling reasons for cytbc_1 complexes residing in lipid-rich domains, with no tight, stoichiometric interaction with another complex such as RC-LH1-PufX. First, strong association of the cytbc_1 with RC-LH1-PufX could lower the number of potential interactions between antenna complexes. Second, cytbc_1 complexes residing in lipid-rich domains are able to utilise quinols from any source such as from Complex I or succinate dehydrogenase rather than those in strongly localised pools. In some bacteria the presence of cytbc_1 complexes in lipid-rich domains might also improve the potential for interacting with the membrane-associated electron carrier cytc_y which is utilised alongside cytc_2 during aerobic and semi-aerobic growth for electron transfer between the *cbb*$_3$-type cyt*c* oxidase and the cytbc_1 complex [45]. A final advantage to residing in a lipid-rich domain may be ready access to a local pool of reduced quinols, in this case fed by turnover at nearby RCs. It is known that quinones form strongly localised pools around sub-populations of RCs to improve the efficiency of quinone reduction [17], so it is therefore not unreasonable to suggest that such pools may also form around the cytbc_1 complexes. Such an arrangement would allow accumulation of quinols during high light growth where reduction of quinone at the RC exceeds the capacity of the cytbc_1 complexes to oxidise them, which occurs at just 5% of full-sunlight intensity [2]. In general, cytbc_1 complexes are the limiting factor in the overall conversion of absorbed solar energy to ATP by *Rba. sphaeroides* [1,2].

The benefits of placing the cytbc_1 complex in a lipid-rich domain may not just be limited to *Rba. sphaeroides*. This theory is supported by the finding that the cytb_6f complex of the model freshwater cyanobacterium *Synechocystis* sp. PCC 6803 is susceptible to SMA

solubilisation, with an efficiency similar to that of the *Rba. sphaeroides* cytbc_1 PSII is similarly affected by SMA. These data support the hypothesis that PSI resides in highly ordered, protein-rich arrays whereas PSII and cytb_6f are likely to reside in less ordered regions of the thylakoid membrane [35]. The *Synechocystis* cytb_6f complex has been described to reside at the "crossroad of photosynthetic electron transport pathways" [18] and thus requires plasticity in terms of its molecular interactions to accept quinols and oxidised cytochrome c_6 or plastocyanin from a variety of sources [18,53,54]. Finally, it is possible that cytb_6f is also found in lipid-rich environments in the thylakoid membranes of chloroplasts; this is supported by the finding of Bell et al. [32] who solubilised spinach thylakoids with SMA and found that the insoluble PSI containing fraction was devoid of cytb_6f and PSII complexes. This suggests that, like in *Synechocystis*, cytb_6f and PSII are susceptible to SMA solubilisation. Johnson et al. [55] have also observed that treatment of spinach thylakoid membranes with the α isomer of DDM specifically removes cytb_6f leaving the PSI and PSII complexes in the membrane, also consistent with a lipid-rich environment for this complex.

5. Conclusion

Using the unique ability of SMA to preferentially solubilise protein complexes from lipid-rich regions of native biological membranes, we have demonstrated that the cytbc_1 complex resides in lipid-rich regions of the otherwise protein-rich chromatophore. These lipid-rich regions have a similar lipid composition to the bulk chromatophore membrane, with around 56 lipids co-purifying with the dimeric cytbc_1 complex. The observation that the insoluble fraction contains large membrane patches of RC-LH1-PufX and LH2, whereas cytbc_1 is purified from the soluble fraction in the form of discrete dimers in small nanodisc structures, further highlights the ability of SMA to remove some complexes from a specific membrane environment whilst preserving protein arrays.

Together these data provide support for the model of chromatophore membranes whereby light-harvesting and RC complexes reside in densely packed arrays for optimal energy transfer efficiency, whereas the cytbc_1 complexes occupy lipid-rich areas [1]. Placing cytbc_1 complexes in lipid-rich domains rather than in arrays or supercomplexes may allow them to accept quinols from a range of electron transport chains to provide both protons and electrons to drive efficient energy generation under a wide-range of growth conditions.

We have extended our study to show that the cytb_6f complex of the cyanobacterium *Synechocystis* is highly susceptible to SMA solubilisation suggesting that it also resides in a locally lipid-rich environment. Our data, along with other published data regarding SMA solubilisation of energy producing membranes, suggest that cytbc_1-type complexes universally reside in lipid-rich membrane regions to aid their critical functions for proton translocation during cellular energy generation under a variety of growth conditions.

Author contributions

DJKS and CNH conceived the study. DJKS, MSP, AH and CNH designed the experiments. DJKS, MSP, AH, MLC, PQ, ECM and PJJ prepared samples, performed experiments and/or analysed data. JM and SPA aided in the preparation of SMA. DJKS, MSP, AH and CNH contributed to preparation of the manuscript.

Transparency document

The Transparency document associated this article can be found, in online version.

Acknowledgments

DJKS, AH, ECM and CNH gratefully acknowledge financial support from the Biotechnology and Biological Sciences Research Council (BBSRC UK), award number BB/M000265/1. CNH was also supported by Advanced Award 338895 from the European Research Council. PQ and PJJ were supported by European Research Council (Advanced Award 338895). MLC was supported by Engineering and Physical sciences Research Council (EPSRC grant EP/I012060/1). MSP was supported by a University of Sheffield doctoral studentship funded by the BBSRC.

Appendix A. Supplementary data

Supplementary data to this article can be found online at https://doi.org/10.1016/j.bbabio.2017.12.005.

References

[1] M.L. Cartron, J.D. Olsen, M. Sener, P.J. Jackson, A.A. Brindley, P. Qian, M.J. Dickman, G.J. Leggett, K. Schulten, C.N. Hunter, Integration of energy and electron transfer processes in the photosynthetic membrane of *Rhodobacter sphaeroides*, Biochim. Biophys. Acta Bioenerg. 1837 (2014) 1769–1780, http://dx.doi.org/10.1016/j.bbabio.2014.02.003 .

[2] M. Sener, J. Strumpfer, A. Singharoy, C.N. Hunter, K. Schulten, Overall energy conversion efficiency of a photosynthetic vesicle, elife 5 (2016) e09541, , http://dx.doi.org/10.7554/eLife.09541 .

[3] S. Kumar, M.L. Cartron, N. Mullin, P. Qian, G.J. Leggett, C.N. Hunter, J.K. Hobbs, Direct imaging of protein organization in an intact bacterial organelle using high-resolution atomic force microscopy, ACS Nano 11 (2016) 126–133, http://dx.doi.org/10.1021/acsnano.6b05647.

[4] A. Hitchcock, C.N. Hunter, M. Sener, Determination of cell doubling times from the return-on-investment time of photosynthetic vesicles based on atomic detail structural models, J. Phys. Chem. B 121 (2017) 3787–3797, http://dx.doi.org/10.1021/acs.jpcb.6b12335.

[5] P.G. Adams, C.N. Hunter, Adaptation of intracytoplasmic membranes to altered light intensity in *Rhodobacter sphaeroides*, Biochim. Biophys. Acta Bioenerg. 1817 (2012) 1616–1627, http://dx.doi.org/10.1016/J.BBABIO.2012.05.013.

[6] J.D. Tucker, C.A. Siebert, M. Escalante, P.G. Adams, J.D. Olsen, C. Otto, D.L. Stokes, C.N. Hunter, Membrane invagination in *Rhodobacter sphaeroides* is initiated at curved regions of the cytoplasmic membrane, then forms both budded and fully detached spherical vesicles, Mol. Microbiol. 76 (2010) 833–847, http://dx.doi.org/10.1111/j.1365-2958.2010.07153.x.

[7] S. Scheuring, R. Nevo, L.-N. Liu, S. Mangenot, D. Charuvi, V. Prima, P. Hubert, J.N. Sturgis, Z. Reich, The architecture of *Rhodobacter sphaeroides* chromatophores, Biochim. Biophys. Acta Bioenerg. 1837 (2014) 1263–1270, http://dx.doi.org/10.1016/j.bbabio.2014.03.011.

[8] M. Chenchiliyan, K. Timpmann, E. Jalviste, P.G. Adams, C.N. Hunter, A. Freiberg, Dimerization of core complexes as an efficient strategy for energy trapping in *Rhodobacter sphaeroides*, Biochim. Biophys. Acta Bioenerg. 1857 (2016) 634–642, http://dx.doi.org/10.1016/j.bbabio.2016.03.020 .

[9] S. Hess, M. Chachisvilis, K. Timpmann, M.R. Jones, G.J. Fowler, C.N. Hunter, V. Sundström, Temporally and spectrally resolved subpicosecond energy transfer within the peripheral antenna complex (LH2) and from LH2 to the core antenna complex in photosynthetic purple bacteria, Proc. Natl. Acad. Sci. U.S.A. 92 (1995) 12333–12337 http://www.pnas.org/content/92/26/12333.abstract.

[10] V. Nagarajan, W.W. Parson, Excitation energy transfer between the B850 and B875 antenna complexes of *Rhodobacter sphaeroides*, Biochemistry 36 (1997) 2300–2306, http://dx.doi.org/10.1021/bi962534b.

[11] P.D. Dahlberg, P.C. Ting, S.C. Massey, M.A. Allodi, E.C. Martin, C.N. Hunter, G.S. Engel, Mapping the ultrafast flow of harvested solar energy in living photosynthetic cells, Nat. Commun. 8 (988) (2017), http://dx.doi.org/10.1038/s41467-017-01124-z.

[12] L.M.P. Beekman, F. van Mourik, M.R. Jones, H.M. Visser, C.N. Hunter, R. van Grondelle, Trapping kinetics in mutants of the photosynthetic purple bacterium *Rhodobacter sphaeroides*: influence of the charge separation rate and consequences for the rate-limiting step in the light-harvesting process, Biochemistry 33 (1994) 3143–3147, http://dx.doi.org/10.1021/bi00177a001.

[13] M.R. Jones, The petite purple photosynthetic powerpack, Biochem. Soc. Trans. 37 (2009) 400–407, http://dx.doi.org/10.1042/BST0370400.

[14] P. Qian, M.Z. Papiz, P.J. Jackson, A.A. Brindley, I.W. Ng, J.D. Olsen, M.J. Dickman, P.A. Bullough, C.N. Hunter, Three-dimensional structure of the *Rhodobacter sphaeroides* RC-LH1-PufX complex: dimerization and quinone channels promoted by PufX, Biochemistry 52 (2013) 7575–7585, http://dx.doi.org/10.1021/bi4011946.

[15] J. Lavergne, A. Verméglio, P. Joliot, Functional coupling between reaction centers and cytochrome bc_1 complexes, in: C.N. Hunter, F. Daldal, M.C. Thurnauer, J.T. Beatty (Eds.), Purple Phototrophic Bact, Springer Netherlands, Dordrecht, 2009, pp. 509–536 , http://dx.doi.org/10.1007/978-1-4020-8815-5_26.

[16] A.R. Crofts, S.W. Meinhardt, K.R. Jones, M. Snozzi, The role of the quinone pool in the cyclic electron-transfer chain of *Rhodopseudomonas sphaeroides*: a modified Q-

cycle mechanism, Biochim. Biophys. Acta 723 (1983) 202–218, http://dx.doi.org/10.1016/0005-2728(83)90120-2.
[17] F. Comayras, C. Jungas, J. Lavergne, Functional consequences of the organization of the photosynthetic apparatus in *Rhodobacter sphaeroides* I. Quinone domains and excitation transfer in chromatophores and reaction center-antenna complexes, J. Biol. Chem. 280 (2005) 11203–11213, http://dx.doi.org/10.1074/jbc.M412088200.
[18] A.N. Tikhonov, The cytochrome b_6f complex at the crossroad of photosynthetic electron transport pathways, Plant Physiol. Biochem. 81 (2014) 163–183, http://dx.doi.org/10.1016/j.plaphy.2013.12.011.
[19] H. Kirchhoff, S. Horstmann, E. Weis, Control of the photosynthetic electron transport by PQ diffusion microdomains in thylakoids of higher plants, Biochim. Biophys. Acta Bioenerg. 1459 (2000) 148–168, http://dx.doi.org/10.1016/S0005-2728(00)00143-2 .
[20] J. Lavergne, P. Joliot, Restricted diffusion in photosynthetic membranes, Trends Biochem. Sci. 16 (1991) 129–134, http://dx.doi.org/10.1016/0968-0004(91)90054-Y .
[21] P. Joliot, J. Lavergne, D. Béal, Plastoquinone compartmentation in chloroplasts. I. Evidence for domains with different rates of photo-reduction, Biochim. Biophys. Acta Bioenerg. 1101 (1992) 1–12, http://dx.doi.org/10.1016/0167-4838(92)90460-U.
[22] D.J.K. Swainsbury, S. Scheidelaar, R. van Grondelle, J.A. Killian, M.R. Jones, Bacterial reaction centers purified with styrene maleic acid copolymer retain native membrane functional properties and display enhanced stability, Angew. Chem. Int. Ed. 53 (2014) 11803–11807, http://dx.doi.org/10.1002/anie.201406412.
[23] J.M. Dörr, M.C. Koorengevel, M. Schäfer, A.V. Prokofyev, S. Scheidelaar, E.A.W. van der Cruijsen, T.R. Dafforn, M. Baldus, J.A. Killian, Detergent-free isolation, characterization, and functional reconstitution of a tetrameric K^+ channel: the power of native nanodiscs, Proc. Natl. Acad. Sci. U. S. A. 111 (2014) 18607–18612, http://dx.doi.org/10.1073/pnas.1416205112.
[24] M. Orwick-Rydmark, J.E. Lovett, A. Graziadei, L. Lindholm, M.R. Hicks, A. Watts, Detergent-free incorporation of a seven-transmembrane receptor protein into nanosized bilayer lipodisq particles for functional and biophysical studies, Nano Lett. 12 (2012) 4687–4692, http://dx.doi.org/10.1021/nl3020395.
[25] K.A. Morrison, A. Akram, A. Mathews, Z.A. Khan, J.H. Patel, C. Zhou, D.J. Hardy, C. Moore-Kelly, R. Patel, V. Odiba, T. Knowles, M.-u.-H. Javed, N.P. Chmel, T.R. Dafforn, A.J. Rothnie, Membrane protein extraction and purification using styrene-maleic acid (SMA) co-polymer: effect of variations in polymer structure, Biochem. J. 473 (2016) 4349–4360, http://dx.doi.org/10.1042/BCJ20160723 .
[26] S. Scheidelaar, M.C. Koorengevel, C.A. van Walree, J.J. Dominguez, J.M. Dörr, J.A. Killian, Effect of polymer composition and pH on membrane solubilization by styrene-maleic acid copolymers, Biophys. J. 111 (2016) 1974–1986, http://dx.doi.org/10.1016/j.bpj.2016.09.025.
[27] D.J.K. Swainsbury, S. Scheidelaar, N. Foster, R. van Grondelle, J. Antoinette Killian, M.R. Jones, The effectiveness of styrene—maleic acid (SMA) copolymers for solubilisation of integral membrane proteins from SMA-accessible and SMA-resistant membranes, Biochim. Biophys. Acta Biomembr. 1859 (2017) 2133–2143, http://dx.doi.org/10.1016/j.bbamem.2017.07.011.
[28] I. Prabudiansyah, I. Kusters, A. Caforio, A.J.M. Driessen, Characterization of the annular lipid shell of the Sec translocon, Biochim. Biophys. Acta Biomembr. 1848 (2015) 2050–2056, http://dx.doi.org/10.1016/j.bbamem.2015.06.024.
[29] S. Gulati, M. Jamshad, T.J. Knowles, K.A. Morrison, R. Downing, N. Cant, R. Collins, J.B. Koenderink, R.C. Ford, M. Overduin, I.D. Kerr, T. Dafforn, A.J. Rothnie, Detergent free purification of ABC transporters, Biochem. J. 461 (2014) 269–278 https://doi.org/10.1042/BJ20131477.
[30] C. Logez, M. Damian, C. Legros, C. Dupré, M. Guéry, S. Mary, R. Wagner, C. M'Kadmi, O. Nosjean, B. Fould, J. Marie, J.A. Fehrentz, J. Martinez, G. Ferry, J.A. Boutin, J.L. Banères, Detergent-free isolation of functional G protein-coupled receptors into nanometric lipid particles, Biochemistry 55 (2016) 38–48, http://dx.doi.org/10.1021/acs.biochem.5b01040.
[31] I.A. Smirnova, D. Sjöstrand, F. Li, M. Björck, J. Schäfer, H. Östbye, M. Högbom, C. von Ballmoos, G.C. Lander, P. Ädelroth, P. Brzezinski, Isolation of yeast complex IV in native lipid nanodiscs, Biochim. Biophys. Acta Biomembr. 1858 (2016) 2984–2992, http://dx.doi.org/10.1016/j.bbamem.2016.09.004.
[32] A.J. Bell, L.K. Frankel, T.M. Bricker, High yield non-detergent isolation of photosystem I-light-harvesting chlorophyll II membranes from spinach thylakoids: implications for the organization of the PS I antennae in higher plants, J. Biol. Chem. 290 (2015) 18429–18437, http://dx.doi.org/10.1074/jbc.M115.663872.
[33] F. Ma, D.J.K. Swainsbury, M.R. Jones, R. van Grondelle, Photoprotection through ultrafast charge recombination in photochemical reaction centres under oxidizing conditions, Philos. Trans. R. Soc. Lond. Ser. B Biol. Sci. 372 (2017), http://dx.doi.org/10.1098/rstb.2016.0378.
[34] A.R. Long, C.C. O'Brien, K. Malhotra, C.T. Schwall, A.D. Albert, A. Watts, N.N. Alder, A detergent-free strategy for the reconstitution of active enzyme complexes from native biological membranes into nanoscale discs, BMC Biotechnol. 13 (2013) 41, http://dx.doi.org/10.1186/1472-6750-13-41.
[35] C. MacGregor-Chatwin, M. Sener, S.F.H. Barnett, A. Hitchcock, M.C. Barnhart-Dailey, K. Maghlaoui, J. Barber, J.A. Timlin, K. Schulten, C.N. Hunter, Lateral segregation of photosystem I in cyanobacterial thylakoids, Plant Cell 29 (2017) 1119–1136, http://dx.doi.org/10.1105/tpc.17.00071.
[36] R. Rippka, J. Deruelles, J.B. Waterbury, M. Herdman, R.Y. Stanier, Generic assignments, strain histories and properties of pure cultures of cyanobacteria, Microbiology 111 (1979) 1–61, http://dx.doi.org/10.1099/00221287-111-1-1 .
[37] D.M. Niedzwiedzki, D.J.K. Swainsbury, E.C. Martin, C.N. Hunter, R.E. Blankenship, Origin of the S^* excited state feature of carotenoids in light-harvesting complex 1 from purple photosynthetic bacteria, J. Phys. Chem. B 121 (2017) 7571–7585, http://dx.doi.org/10.1021/acs.jpcb.7b04251.
[38] D.M. Niedzwiedzki, P.L. Dilbeck, Q. Tang, E.C. Martin, D.F. Bocian, C.N. Hunter, D. Holten, New insights into the photochemistry of carotenoid spheroidenone in light-harvesting complex 2 from the purple bacterium *Rhodobacter sphaeroides*, Photosynth. Res. 131 (2017) 291–304, http://dx.doi.org/10.1007/s11120-016-0322-2.
[39] M. Rögner, P.J. Nixon, B.A. Diner, Purification and characterization of photosystem I and photosystem II core complexes from wild-type and phycocyanin-deficient strains of the cyanobacterium *Synechocystis* PCC 6803, J. Biol. Chem. 265 (1990) 6189–6196 http://www.jbc.org/content/265/11/6189.abstract.
[40] D.W. Dorward, Detection and quantitation of heme-containing proteins by chemiluminescence, Anal. Biochem. 209 (1993) 219–223, http://dx.doi.org/10.1006/abio.1993.1110 .
[41] M.D. Abràmoff, P.J. Magalhães, S.J. Ram, Image processing with ImageJ, Biophoton. Int. 11 (2004) 36–41, http://dx.doi.org/10.1117/1.3589100 .
[42] M. Tichý, M. Bečková, J. Kopečná, J. Noda, R. Sobotka, J. Komenda, Strain of *Synechocystis* PCC 6803 with aberrant assembly of photosystem II contains tandem duplication of a large chromosomal region, Front. Plant Sci. 7 (2016) 648 https://www.frontiersin.org/article/10.3389/fpls.2016.00648.
[43] M. Dezi, F. Francia, A. Mallardi, G. Colafemmina, G. Palazzo, G. Venturoli, Stabilization of charge separation and cardiolipin confinement in antenna-reaction center complexes purified from *Rhodobacter sphaeroides*, Biochim. Biophys. Acta Bioenerg. 1767 (2007) 1041–1056, http://dx.doi.org/10.1016/j.bbabio.2007.05.006.
[44] M. Contin, S. Lucangioli, M. Martinefski, S. Flor, V. Tripodi, Miniaturized HPLC-UV method for analysis of coenzyme Q10 in human plasma, J. Liq. Chromatogr. Relat. Technol. 34 (2011) 2485–2494, http://dx.doi.org/10.1080/10826076.2011.591028.
[45] H. Myllykallio, D. Zannoni, F. Daldal, The membrane-attached electron carrier cytochrome c_y from *Rhodobacter sphaeroides* is functional in respiratory but not in photosynthetic electron transfer, Proc. Natl. Acad. Sci. U. S. A. 96 (1999) 4348–4353, http://dx.doi.org/10.1073/pnas.96.8.4348.
[46] M. Elberry, K. Xiao, L. Esser, D. Xia, L. Yu, C.A. Yu, Generation, characterization and crystallization of a highly active and stable cytochrome bc_1 complex mutant from *Rhodobacter sphaeroides*, Biochim. Biophys. Acta Bioenerg. 1757 (2006) 835–840, http://dx.doi.org/10.1016/j.bbabio.2006.05.031.
[47] L. Esser, M. Elberry, F. Zhou, C.A. Yu, L. Yu, D. Xia, Inhibitor-complexed structures of the cytochrome bc_1 from the photosynthetic bacterium *Rhodobacter sphaeroides*, J. Biol. Chem. 283 (2008) 2846–2857, http://dx.doi.org/10.1074/jbc.M708608200.
[48] R. Cuevas Arenas, B. Danielczak, A. Martel, L. Porcar, C. Breyton, C. Ebel, S. Keller, Fast collisional lipid transfer among polymer-bounded nanodiscs, Sci. Rep. 7 (2017) 45875, http://dx.doi.org/10.1038/srep45875.
[49] G. Hazell, T. Arnold, R.D. Barker, L.A. Clifton, N.J. Steinke, C. Tognoloni, K.J. Edler, Evidence of lipid exchange in styrene maleic acid lipid particle (SMALP) nanodisc systems, Langmuir 32 (2016) 11845–11853, http://dx.doi.org/10.1021/acs.langmuir.6b02927.
[50] C. Poggese, P. Polverino de Laureto, G.M. Giacometti, F. Rigoni, R. Barbato, Cytochrome b_6/f complex from the cyanobacterium *Synechocystis* 6803: evidence of dimeric organization and identification of chlorophyll-binding subunit, FEBS Lett. 414 (1997) 585–589, http://dx.doi.org/10.1016/S0014-5793(97)01078-8.
[51] S.S. Hasan, W.A. Cramer, Internal lipid architecture of the hetero-oligomeric cytochrome b_6f complex, Structure 22 (2014) 1008–1015, http://dx.doi.org/10.1016/j.str.2014.05.004.
[52] J. Broecker, B.T. Eger, O.P. Ernst, Crystallogenesis of membrane proteins mediated by polymer-bounded lipid nanodiscs, Structure 25 (2017) 384–392, http://dx.doi.org/10.1016/j.str.2016.12.004.
[53] L.N. Liu, Distribution and dynamics of electron transport complexes in cyanobacterial thylakoid membranes, Biochim. Biophys. Acta 1857 (2016) 256–265, http://dx.doi.org/10.1016/j.bbabio.2015.11.010.
[54] D.J. Lea-Smith, P. Bombelli, R. Vasudevan, C.J. Howe, Photosynthetic, respiratory and extracellular electron transport pathways in cyanobacteria, Biochim. Biophys. Acta Bioenerg. 1857 (2016) 247–255, http://dx.doi.org/10.1016/j.bbabio.2015.10.007.
[55] M.P. Johnson, C. Vasilev, J.D. Olsen, C.N. Hunter, Nanodomains of cytochrome b_6f and photosystem II complexes in spinach grana thylakoid membranes, Plant Cell 26 (2014) 3051–3061 www.plantcell.org/cgi/doi/10.1105/tpc.114.127233.